Int. J. Electrochem. Sci., 14 **(2019)** 7047 – 7061, doi: 10.20964/2019.08.90

International Journal of
ELECTROCHEMICAL
SCIENCE
www.electrochemsci.org

Electrochemical study on Surface Oxidation of Natural Pyrite in Ferric Sulfate Solution

Guobao Chen, Hongying Yang

School of Metallurgy, Northeastern University, Shenyang 110819, Liaoning, China
E-mail: chengb@smm.neu.edu.cn

Received: 10 March 2019 / *Accepted:* 10 May 2019 / *Published:* 30 June 2019

Surface oxidation of natural massive pyrite in 0.5 M sulfuric acid solutions with different ferric concentrations was investigated. The electrode of natural pyrite was made and its behavior was measured using cyclic voltammetry (CV), linear sweep voltammetry (LSV) and rotating disk electrode (RDE). According to the test results, the open circuit potential (OCP) of pyrite grew steadily when the ferric concentration increased. Furthermore, the rate of pyrite oxidation was strengthened with the addition of ferric ions. However, it is difficult to distinguish the chemical or electrochemical oxidation on pyrite and their interaction process. Here, the electron transferred numbers (ETNs) of oxidation processes on pyrite were calculated. And it is found the ETN could be a useful tool to compare rapidly the oxidation reactivity for different conditions. The overall surface oxidation process on pyrite occurred in the potential range of -0.450 V to 0.050 V vs. AgCl/Ag. The average ETN for pyrite oxidation was around 2 in sulfuric acid. The increasing of ferric ion was found to affect ETN markedly while the polarization current was raised, which indicate that the pyrite electrochemical oxidation was inhibited by adding ferric ions, and the dissolution was the main result of chemical oxidation. Moreover, the studies of the surface oxidation on pyrite with adding silver ion and that on chalcopyrite were also conducted to confirm the new founds. Silver ion is inferred to be difficult to form silver atoms and influence the oxygen electrochemical oxidation less.

Keywords: Surface oxidation; Pyrite; Rotating disc electrode; Electron transferred numbers; Ferric ion

1. INTRODUCTION

Pyrite (FeS_2, iron disulfide) is commonly associated with other base metal sulfide minerals (e.g., galena, sphalerite, chalcopyrite), and also the most prevalent gold-carrying mineral. [1-3]. Since pyrite is one of the major minerals on earth, its oxidation is an important process not only in the geochemical iron and sulfur circulations but also in industrial mineral beneficiation processes and its oxidative leaching reactions [4, 5]. Oxidation can improve the hydrophobicity of pyrite surface and thus change

the interaction between the mineral particles and flotation collectors. Pyrite oxidation is also a primary process in the leaching process of metal sulfides. Moreover, the oxidation of exposed pyrite can cause the release of large amounts of iron, sulfate, protons and further potentially toxic trace metals into water. It is a cause of drainage, known as acid mine drainage, which may cause an environmental problem. Besides, researchers are making progress in non-noble-metal catalysts using pyrite-type minerals including pyrites, molybdenites, bismuthinite, pentlandite, and others. They are currently experiencing an intensified interest [6].

Previous studies of pyrite oxidation mechanisms have been conducted and used to estimate the influence factors for pyrite oxidation kinetics. Several oxygen consumption reactions at the pyrite surface have been put forward. The pyrite reacts with dissolved O_2 in water can form ferrous iron, sulfate, and acid according to the following reaction [7-9]:

$$2FeS_2 + 7O_2(aq) + 2H_2O \rightarrow 2Fe^{2+} + 4SO_4^{2-} + 4H^+ \quad (1)$$

$$4Fe^{2+} + O_2(aq) + 4H^+ \rightarrow 4Fe^{3+} + 2H_2O \quad (2)$$

$$FeS_2 + 14Fe^{3+} + 8H_2O \rightarrow 15Fe^{2+} + 2SO_4^{2-} + 16H^+ \quad (3)$$

The ferrous ion produced will continue to be oxidized to ferric ion by oxygen (Eq. (2)). The dissolved molecular oxygen and ferric ion are recognized as the two most principal oxidizing agent for pyrite dissolution (Eq. (1) and Eq. (3)). However, these reactions of overall processes do not take account of other elementary steps that form various intermediate species observed. The electron transfer rate of production or dissolution for these surface layers can hardly be tested, thus monitoring pyrite oxidation still have significance and the surface oxidation kinetics of pyrite in different media is far from being clarified.

The former researches have mainly reported that the existence of oxygen and Fe^{3+} can notably enhance the rate of pyrite dissolution and that ferric ion can obtain more effective than the dissolved O_2 within all pH range, however, pyrite dissolution will not carry on if the dissolved oxygen in the solution are consumed out [9]. According to isotope studies, with low ferric ion/pyrite surface ratios, a significant proportion of molecular oxygen in sulfate absorbed onto the pyrite surface acted as pyrite oxidant and it worked only (or at least predominantly) in the presence of water [10]. There are various influence factors of pyrite oxidation, among these sulfuric acid product was considered making a great contribution to the environmental problem of acid rock drainage. Besides, the growing pH value will speed up pyrite oxidation [9, 10]. The redox potential (Eh) also presented the predominant effects and pyrite leaching rate was shown quite faster at a potential of 900 mV (SHE) than at 700 mV, when HCl, H_2SO_4 and $HClO_4$ were applied as the leaching media [9]. Most of the proposed pyrite oxidation mechanisms are based on these experimental data. Some of them tried to find a promising approach to suppress the pyrite oxidation on a basis of presenting the oxidative kinetics of pyrite itself [11], while others are majored in the reductive reaction of involved oxidants during the mineral leaching processes [10]. A number of characterization techniques have been applied to examine the oxidized pyrite, for examples, X-ray diffraction (XRD), scanning photoelectron microscopy (SPEM), ultraviolet photoelectron spectroscopy (UPS), X-ray photoemission electron microscopy (PEEM), scanning tunnelling microscopy (STM), X-ray absorption (XAS), and so on [1, 12]. The oxidation products of pyrite in the aqueous solution are various and complex. The dominant product is sulfate while other by-products also can be formed, for

instance, ferric hydroxide precipitate, polysulfide, elemental sulfur, iron (III) oxyhydroxide, hydrogen sulfide gas, and iron oxide. Furthermore, several intermediates can also be produced, such as sulfite, thiosulfate and polythionates. Lots of previous researches have put forward the oxidation mechanism that sulfate is finally formed and ferrous iron is released after experiencing a complex multiple step disulfide oxidation process, which involving a number of charge transfers and several intermediates. However, there is still lack of an efficient method to distinguish these multiple steps up to now, and the effect of solution conditions on the electron transfer process between the oxidants and pyrite is difficult to quantify. Therefore, the process conditions are usually set mindlessly and cannot meet the needs. For example, the dissolved oxygen requirement during the process operation cannot be ensured by taking effective adjustment and control measures. Before the overall oxidation mechanism of pyrite are fully understood and grasped, an urgent matter is to identify the interaction the interaction between electrochemical and chemical oxidation. Since the pyrite oxidation started from the dissolved oxygen reduction reactions in the water, it is more practicable to study the reaction products influence the electrochemical oxidation of pyrite in acidic media.

Thus this study is aimed to figure out the properties of surface oxidation on pyrite in sulfuric acid, and investigate the influence of adding a different amount of ferric ions in the solution, with the main electrochemical techniques such as cyclic voltammetry (CV) and linear sweep voltammetry (LSV). The open circuit potentials and the tafel slopes for various iron content were also obtained. Furthermore, to make a more quantitative evaluation of ferric ions effect on the dissolved oxygen reduction reaction involved during the dissolution process, rotating disc electrodes were made with the natural massive pyrite samples. Finally, from the electrochemical measurement results, the electron transfer numbers have been calculated and compared for different conditions.

2. MATERIALS AND METHODS

2.1 Pyrite sample preparation

A pyrite specimen obtained from Dabaoshan polymetallic sulphide ore of China was applied as a work electrode material in this study. The chemical composition of the raw pyrite sample can be analyzed by using X-ray fluorescence (XRF). Analysis is also made on the crystallinity of pyrite by means of X-ray diffraction (XRD), which conducted by using an X'Pert Pro multifunction diffractometer, which is produced by Panalytical (Holland) in the service of 40 mA and 40 kV, the scanning rate was 0.2 °/s and the detection ranged from 5° to 90°. From the test results, the purity of the pyrite sample is 97.35%, and the major impurity in the sample is silica (2.48%). The obtained XRD pattern is shown in Figure 1, it is easy to learn that the diffraction peaks fit well comparing to the standard pyrite XRD pattern (PDF 00-042-1340), and the diffraction peaks of SiO_2 were barely visible. It also can be confirmed that there are no other impurity phases, such as ferrous sulphide from this XRD pattern.

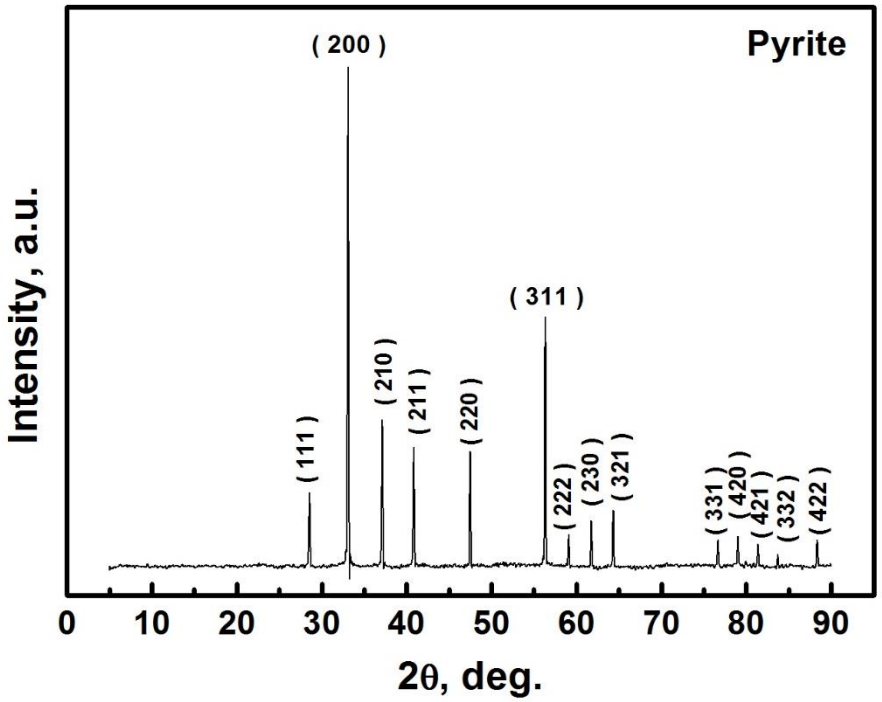

Figure 1. XRD pattern of the natural pure FeS_2 sample.

2.2 Electrochemical electrode materials

In order to apply the rotating disk electrode measurements, the massive pyrite samples were designed as the cylinders and cut by a diamond saw blade first of all. The collective surface area of pyrite electrodes exposed to the solution environment were set at 0.2374 cm^2. Considering the semiconducting properties of pyrite, the thickness of electrode materials were controlled at 1 cm. After that, the cylinder specimens were cleaned by using double-distilled water and analytical grade acetone for three times each. When the samples were dried, they were bonded to the highly conductive copper bars by means of silver-epoxy adhesive (Dotite®, D-550). Then the prepared samples were put into the PTFE tubes and their interspaces are filled and sealed with epoxy resin (Epofix®, Struers). To remove the surface impurities deeply and activate the electrode, a wet mechanical polishing using the silicon carbide papers (grit sizes 600, 1000 and 1200) were conducted in turn. An optical microscope has also been applied to examine each polished sample surface to ensure the best repeatability of experiments. That is, the surface state on each fresh polished pyrite should be very close to the previous one observed, and there is no cracked or broken. Finally, the electrode materials were cleaned by deionized water several times, and dried at 60 ℃ in a vacuum oven for 12 hours.

2.3 Electrochemical electrolyte solutions

Analytical grade reagents and deionized water (>17.5 mΩ) were used to prepare all electrolyte solutions in the experiments. The primary supporting electrolyte solutions were sulfuric acid (H_2SO_4, Fisher Scientific, dissolving reagent grade), and the concentration of the sulfuric acid solutions was kept

at 0.5 M. Ferric sulfate pentahydrate ($Fe_2(SO_4)_3 \cdot 5H_2O$, 97%, Fisher Scientific) were used as an iron source, the additions of ferric ion in the electrolytes were 0, 0.05, 0.10, 0.50 and 10 g/L, respectively. To compare the pyrite oxidation behavior in the solutions containing ferric iron, the solution with 0.10 g/L silver ion from silver nitrate ($AgNO_3$, analytically pure grade, Fisher Scientific) was also prepared.

2.4 Electrochemical measurements

The electrochemical measurement system consisted of three electrodes, the prepared pyrite cylinder electrodes were always used as the work electrodes, an Ag/AgCl/KCl (3.0 mol/L) electrode was served as a reference electrode, and the platinum wire (99.999%, Alfa Aesar) was applied as the auxiliary electrode. The tests were carried out on a potentiostat/galvanostat 273A electrochemical work station (EG&G Princeton Applied Research, USA) controlled by software Powersuite. Ultra high purity N_2 and O_2 gas (99.999% and low hydrocarbons) was purged into the electrolyte solution according to the need of experiments. The electrolyte volume was kept constant at 1000 mL during the whole tests and the electrolytic cell was placed in a water bath to maintain the temperature at 25 °C. Besides, a Luggin capillary probe connected the reference electrode to the electrolyte was introduced to get more precise results. Potentials and currents results were recorded by the software.

Gases (N_2 or O_2 gas, 99.999%) were blown into the electrolyte solutions at a fixed flow rate for at least twenty minutes, before the electrochemical measurement got started. The oxidation behavior on natural massive pyrite were enclosed by the electrochemical techniques such as CV, LSV and RDE. The polarization potential range for newly polished pyrite electrodes were all from 1.0 to -0.6 V vs. AgCl/Ag during the CV and LSV experiments, while the scan rates for the two electrochemical tests were respectively 20 mV/s and 2 mV/s. The scanned potential range for the RDE tests were from 0.5 V to -0.5 V vs. AgCl/Ag at a fixed scanned rate 2 mV/s. The rotating rate varied between 100 and 2500 rpm. To ensure the accuracy of the results, the fresh pyrite working electrodes were soaked in the electrolyte to be measured for at least twenty minutes.

3. RESULTS AND DISCUSSION

3.1 Cyclic voltammetry study

The potential measurements in previous reports usually focus on the potential range above 0.50 V, which is considered being relevant to pyrite oxidation. However, the first electron acceptor in the overall reaction is the dissolved oxygen on the pyrite surface. Thus the oxidation behavior of the natural pyrite mineral measured by cyclic voltammetry should be examined using a wide potential window.

When the working electrode was stabilized for above twenty minutes, the open circuit potential (OCP) was carefully observed until the potential varied within ± 2 mV. The cyclic voltammetry scan was performed from the OCP at a scan rate of 20 mV/s. The potential range was $-0.600\ V \leqq E \leqq 1.00\ V$ vs. AgCl/Ag, and the electrolyte was not stirred during the scanning process.

The CV tests of the pyrite electrodes in O_2 saturated 0.5 M H_2SO_4 solutions were first studied at 25 ℃, comparing with those in N_2 saturated 0.5 M H_2SO_4 solutions. For the two different gases saturated

solutions, the OCP were recorded to be 0.344 V and 0.242 V vs. AgCl/Ag respectively. The increased OCP may be due to the adsorption molecular oxygen [13]. As shown in Figure 2, it is observed that the pyrite CV curve shows two anodic peaks (A1 and A2) and two cathodic peaks (C1 and C2). The former peaks A1 and A2 were not prominent as the two catholic peaks. The potential ranges of these peaks were figured out, and they were 0.300 ≦ E_{A1} ≦ 0.650 V, -0.300 V ≦ E_{A2} ≦ 0.050 V, 0.200 V ≦ E_{C1} ≦ 0.600 V, -0.450 V ≦ E_{C2} ≦ 0.050 V (vs. AgCl/Ag) respectively. The cathodic peak C1 found in the positive scan in the former researches is always attributed to the reduction of the surface species formed (Eq. (4) and (5)) [14].

$$FeS_2 + 11H_2O \rightarrow Fe(OH)_3 + 2SO_4^{2-} + 19H^+ + 15e^- \quad (4)$$

$$Fe(OH)_3 + 3H^+ + e^- \rightarrow Fe^{2+} + 3H_2O \quad (5)$$

The involvement of the oxidisable intermediate products, such as metal-deficient sulfides and thiosulfate, were considered being relevant to the results at lower potentials. The new phases were believed to exist in pyrite oxidation process in acidic media [15, 16]. Thus some researches proposed that the cathodic current peak C2 is ascribed to the reduction of pyrite to form FeS and H_2S (Eq. (6)). However, there is a lack of direct evidence to prove the reaction at that potential.

$$FeS_2 + 2H^+ + 2e^- \rightarrow FeS + H_2S \quad (6)$$

Here, the cathodic peak C2 is supposed to the reduction reaction of the absorbed oxygen on the pyrite surface (Eq. (7)), since the dissolved oxygen is more prone to accept electron than the intermediate products. Besides, an amount of previous reports have proved the dissolved oxygen as an effective oxidant for pyrite.

$$4H^+ + O_2 + 4e^- \rightarrow 2H_2O \quad (7)$$

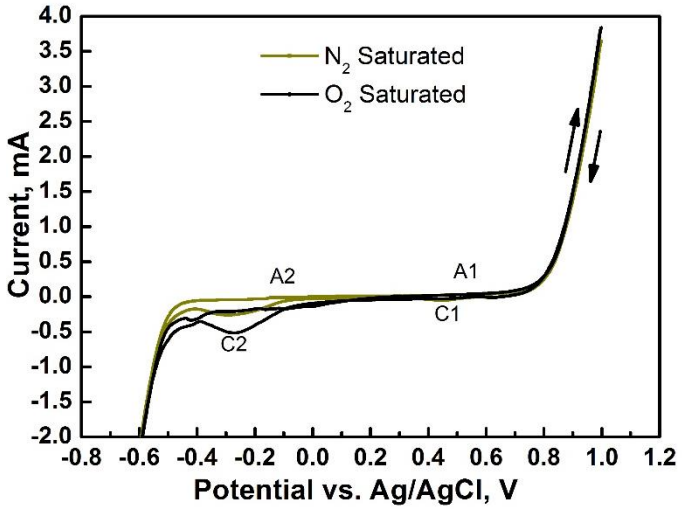

Figure 2. Cyclic voltammograms for the oxidation behavior of a pyrite electrode in solutions of 0.5 M H_2SO_4 with N_2 and O_2 saturated respectively at a scan rate of 20 mV/s. The temperatures was controlled at 25 °C.

It is obvious that the current peak C2 for pyrite electrode in solution saturated by oxygen shows larger than that solution saturated by nitrogen as expected. It can be considered as indicative differences in behavior, which inferred to the increasing concentration of the dissolved oxygen on pyrite surface.

Therefore, the anodic current peaks A1 and A2 were proposed to the results of the oxidation of pyrite and the activation of intermediate surface product, respectively.

The pyrite CV curves for the electrolyte with various ferric ions (from 0 to 10 g/L) adding into 0.5 M H_2SO_4 saturated by oxygen were also shown in Figure 3. The OCPs for the surface oxidation on pyrite samples were measured to be 0.344 V, 0.447 V, 0.460 V, 0.487 V and 0.498 V vs. AgCl/Ag for the addition of ferric ions 0, 0.05, 0.10, 0.50 and 10 g/L, respectively. There are four peaks named as A1, A2, C1 and C2, the potential regions of which are similar wide to the former ones in Fig. 2. However, the peak currents owed a great change when the concentration of ferric ions in the electrolyte solution increased. The anodic current peak C1 and reduction peak A1 were more and more identifiable when the iron content of the solution went up from 0 to 0.50 g/L. The potential difference between the peaks C1 and A1 was stayed at 140 mV until the ferric ion content was larger than 0.50 g/L. After the ferric ion concentration were increased to 10 g/L, the potential difference was rapidly expanded to nearly 300 mV. This was inferred to the reduction-oxidation reaction of pyrite dissolution (Eq. (4) and (5)), what is more important, it is also the result of the ferric ion reduction and ferrous oxidation coming from the solution near to the pyrite sample surface (Eq. (8)), which differs from the other reports.

$$Fe^{3+} + e^{-} \rightarrow Fe^{2+} \qquad (8)$$

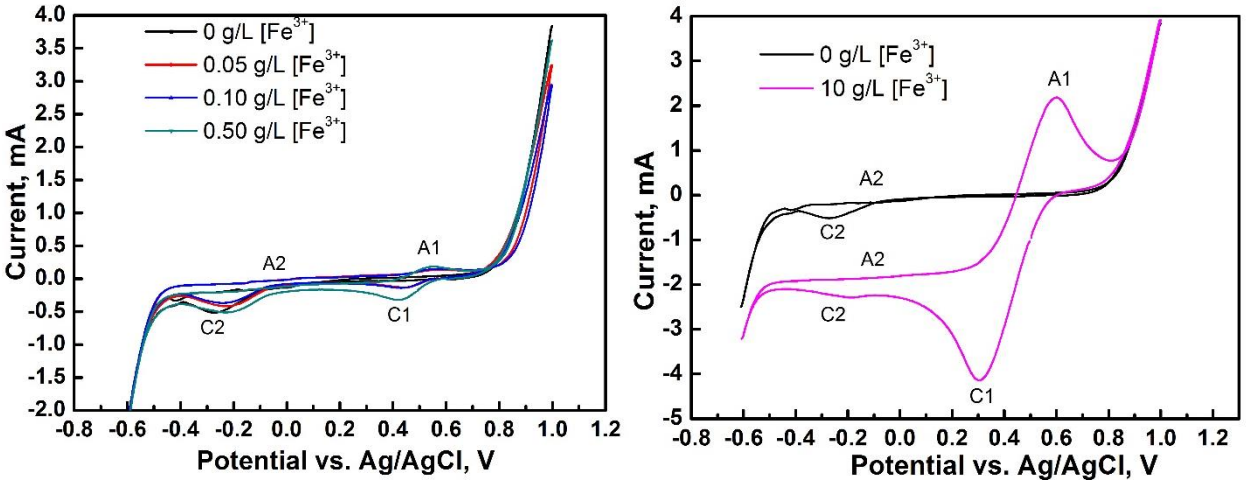

Figure 3. Cyclic voltammograms for the oxidation behavior of a pyrite electrode in solutions of O_2 saturated 0.5 M H_2SO_4 with the addition of ferric ions at a scan rate of 20 mV/s. The concentration of ferric ions varied from 0 to 10 g/L, the temperatures was controlled at 25 °C.

It is interesting to find that there was not so different for C2/A2 peaks when the content of ferric ions rising. The anodic current peak C2 and reduction peak A2 had more stable potential ranges when the iron contents raised from 0 to 10 g/L. This implies that the reactions occurring at the potentials range from -0.450 V to 0.050 V (vs. AgCl/Ag) are not ferric-ion dependent reactions. Since ferric ions are strong oxidants, sulfur atoms and thiosulfate ions on the pyrite surface would be oxidized (Eq. (3), Eq. (9) and (10)) [16], these reactions current should be enhanced obviously with the addition of ferric ions. Therefore, the peaks C2 and A2 can be confirmed as the reduction reaction of dissolved oxygen and water oxidation reaction respectively as mentioned above.

$$S + 4H_2O + 6Fe^{3+} \rightarrow 6Fe^{2+} + 2HSO_4^{-} + 8H^{+} \qquad (9)$$

$$S_2O_3^{2-} + 5H_2O + 8Fe^{3+} \rightarrow 8Fe^{2+} + 2HSO_4^- + 8H^+ \quad (10)$$

3.2 Polarization measurements

Current-potential curves measurements were conducted at a rate of 2 mV/s, by changing the electrode potentials from 1.00 V to -0.600 V vs. AgCl/Ag. Before each experiment, the rotating pyrite electrodes was immersed and equilibrated in the solution for not less than 20 min to assure steady states. The polarization measurements were performed with a rotating speed at 400 rpm.

The LSV measurements results for pyrite rotating electrodes in N_2- and O_2- saturated 0.5 M H_2SO_4 respectively were presented in Fig. 4(a). Polarization parameters for pyrite electrodes were listed in table 1. It is interesting to infer that the shapes of anodic curves with different gases bubbled were quite similar, confirmed the CV result in Fig. 2 that the peaks C1 and A1 changed less. In contrast, the cathodic curves differed and their tafel slopes (b_c) were obtained 0.354 and 0.829 V decade^{-1} for the solutions saturated by O_2 and N_2, respectively. And the corrosion potentials for these two electrolyte solutions were 0.551 V and 0.543 V vs. AgCl/Ag respectively, indicating that pyrite mineral is stable in acidic media.

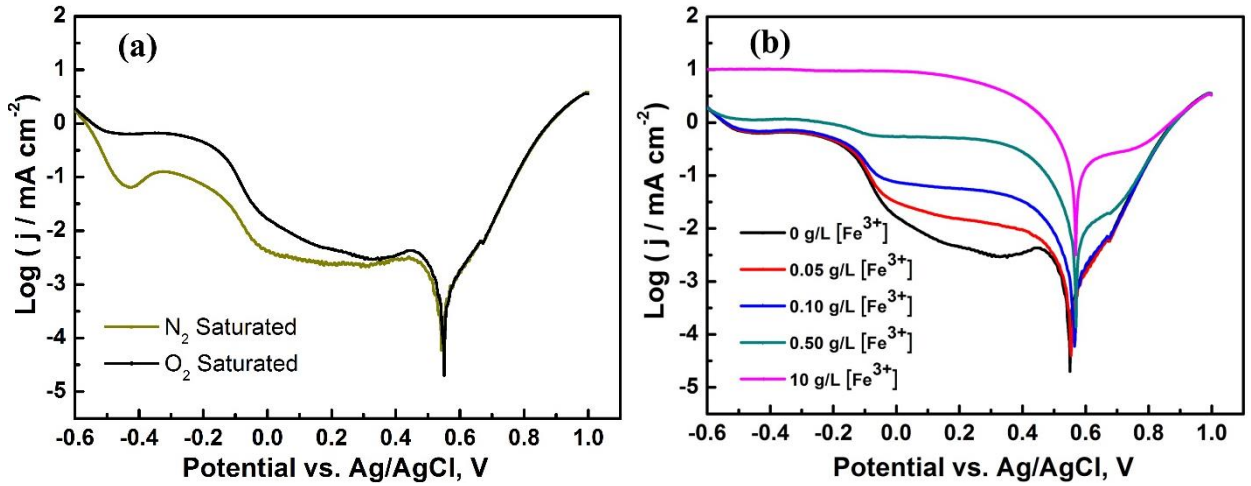

Figure 4. (a) Polarization curves for pyrite rotating electrodes in 0.5 M H_2SO_4 saturated by N_2 and O_2 respectively; (b) Polarization curves for pyrite rotating electrodes in 0.5 M H_2SO_4 saturated by pure oxygen and added various ferric ions, the ferric ions contents were 0, 0.05, 0.10, 0.50 and 10 g/L respectively. Conditions: temperature, 25 °C; rotating speed, 400 rpm; sweep rate, 2 mV/s.

Figure 4(b) shows polarization curves for pyrite electrodes in 0.5 M H_2SO_4 saturated by O_2 with the addition of various ferric ion contents. The corrosion currents and potentials (j_{corr} and E_{corr}), the anodic and cathodic tafel slopes (b_a and b_c) were obtained from the curves and presented in table 1. From the measurement results, it can be observed that the cathodic current affected more significantly with the potential range from -0.200 V to 0.400 V vs. AgCl/Ag when the ferric ion added. This may be ascribed to the two reduction processes on pyrite surface, and the current is reflecting the overall reduction rate of oxygen and ferric ions [17]. It has also been inferred that with the ferric ion content increasing from 0 to 10 g/L, the values of corrosion currents and potentials, the anodic and cathodic tafel slopes all rose

alongside. The growth rate of the cathodic tafel slopes were obviously bigger than that of anodic tafel slopes, indicating that with the ferric ion content growing, the reduction reaction of dissolved oxygen on the natural pyrite got more and more difficult according to the analysis above. The enhancing oxidation rate of pyrite is thus inferred as the main effect of the increasing reaction rate of ferric ions. From results listed in table 1, it also can be learned that the corrosion potentials varied less than 30 mV with the addition of ferric ions, which means that the corrosion potential of pyrite cannot be improved by ferric ion in acidic media.

Table1. Polarization parameters for pyrite electrodes in 0.5 M H_2SO_4 solutions saturated by O_2 with different concentration of ferric ions.

Ferric ion contents / g L^{-1}	j_{corr} / μA cm^{-2}	E_{corr} / V vs. AgCl/Ag	b_a / V dec^{-1}	b_c / V dec^{-1}
0	0.020	0.551	0.113	-0.354
0.05	0.040	0.554	0.117	-0.855
0.10	0.060	0.565	0.128	-1.73
0.50	0.140	0.570	0.246	-6.29
10	3.181	0.568	0.766	-8.04

3.3 Rotating disk electrode study

Cyclic voltammetry and polarization curves were all related to the overall reaction processes and the two oxidation behaviors on pyrite surface still need to be distinguished more clearly. Since the redox reaction for ferric ions involved the chemical oxidation of pyrite, the study of dissolved oxygen reduction reaction is more available. It is widely agreed that in acid medium there are two reaction pathways [18]: the one is the dissolved oxygen accepts four and generates water directly (Eq. (11)); the other one is that the oxygen firstly forms hydrogen peroxide by capturing two electrons (Eq. (12)), the intermediate product eventually changes to water with absorbing two another electrons (Eq. (13)).

$$4H^+ + O_2 + 4e^- \rightarrow 2H_2O \qquad E_0 = 1.229 \text{ V vs.NHE} \qquad (11)$$

$$2H^+ + O_2 + 2e^- \rightarrow 2H_2O_2 \qquad E_0 = 0.67 \text{ V vs.NHE} \qquad (12)$$

$$2H^+ + H_2O_2 + 2e^- \rightarrow 2H_2O \qquad E_0 = 1.77 \text{ V vs.NHE} \qquad (13)$$

The RDE experiments were carried out to verify and utilize the principles of oxygen reduction reaction on natural mineral surface. In order to make the quantitative analysis, Koutecky–Levich equation as followed has been applied to calculate the numbers of electrons transferred for each oxygen molecule occurred on pyrite surface [19].

$$-\frac{1}{J} = \frac{1}{J_k} + \frac{1}{0.62nFAD^{2/3}cv^{-1/6}\omega^{1/2}} \qquad (14)$$

where J_k is the overall kinetic current; F is Faraday constant (96,485 C mol^{-1}); n is the number of electron transferred for the overall reduction reaction; c is the saturation concentration of dissolved oxygen in 0.5 M aqueous- H_2SO_4 at 25 °C (1.13×10^{-6} mol cm^{-3}); A is the contact area of the pyrite rotating electrode (0.2374 cm^{-2}); ω is the sample rotation rate; D is the diffusion coefficient for the

dissolved O_2 in electrolyte solution (1.93×10^{-5} cm^2 s^{-1}); v is the kinematic viscosity of the reaction system (9.5×10^{-3} cm^2 s^{-1}) [20].

RDE test results were shown in Fig. 5 for the reduction reaction of dissolved oxygen on pyrite rotating electrode in O_2 -saturated 0.5 M H_2SO_4 with a scan rate at 2 mV/s, the ferric ion content in the electrolyte were 0, 0.05, 0.10, 0.50 and 10 g/L, respectively. Besides, the corresponding Koutecky-Levich plots were also displayed at various potentials: 0 mV, -50 mV, -100 mV and -150 mV respectively, with the rotating rates differing from 100 to 2500 rpm. It is apparent that there is a linear interrelationship between the J^{-1} and $\omega^{-1/2}$ at whole investigated potentials. However, with the addition of ferric ions in the electrolyte, these plots gradually lose parallelism and are hard to obtain the similar slopes. It can be inferred that the reduction reaction of dissolved oxygen influenced a lot by the ferric ion. The chemical oxygen may disturb electrochemical reaction and result in the insufficient reduction of oxygen to final product. It is also worth noting that there is no obvious oxygen reduction peak when the ferric ion concentration in the electrolyte rose to 10 g/L, differing from the others. As analyzed above, ferric ion will slow down the oxygen reduction process on pyrite surface.

The electron transfer numbers of oxygen reduction were calculated by applying the Eq. (14) on a basis of the K-L plots. The relationship between (n) and the scan potentials were also examined and presented in in Fig. 6. It is easy to learn that when the ferric ion contents range from 0 to 0.50 g/L, the electron transfer numbers declined constantly with the increasing potentials from -150 to 0 mV vs. AgCl/Ag. This may be caused by that at lower overpotential (such as 0 mV vs. AgCl/Ag), the electrochemical reduction of oxygen are more primary reactions, while at high overpotential (such as -150 mV vs. AgCl/Ag) the reaction processes will induced by several other processes (such as diffusion process), which enhancing the electron transfer numbers.

The average transferred electron number for dissolved oxygen reduction was calculated 2.10 in sulfuric acid with no ferric ion added. Thus it is inferred that the oxygen on pyrite surface experiences a two-electron reduction pathway (Eq. (12)). It is also easily found that the ETN changed from 7 to 2 when the addition of ferric ions increased from 0 to 0.50 g/L, illustrating that the electron transfer process is affected dramatically by the ferric ion contents in the electrolyte. The chemical oxidant will influence the electrochemical oxidation process.

In previous researches, the 4-electron reduction is always considered more efficient than the 2-electron reduction. However, the more transferred electrons means the higher barrier need to be overcome and the reactions are more difficult to proceed. The inner-sphere electron transfer mechanism was proposed to explain the reduction of dissolved oxygen on pyrite mineral surface. The less ETNs caused by the formation of reaction intermediates (i.e., peroxide) obtain the higher reaction speed based on the lower equilibrium potential (Eq. (11-13)). However, ferric ion will affect the continuing reduction of oxygen, since the intermediate compounds are always unstable. For instance, the Fenton-like reaction will start with the addition of ferric ions (Eq. (15-17)) [21, 22]. What makes the matter worse is that, the reversible reaction, oxidation of the intermediates may occur due to the increasing of ferric ion content. Finally, these reversible reactions made the ETNs increasing.

$$H_2O_2 + Fe^{3+} \rightarrow FeOOH^{2+} + H^+ \quad (15)$$

$$FeOOH^{2+} \rightarrow Fe^{3+} + \bullet OH \quad (16)$$

$$Fe^{3+} + \bullet OOH \rightarrow Fe^{2+} + O_2 + H^+ \quad (17)$$

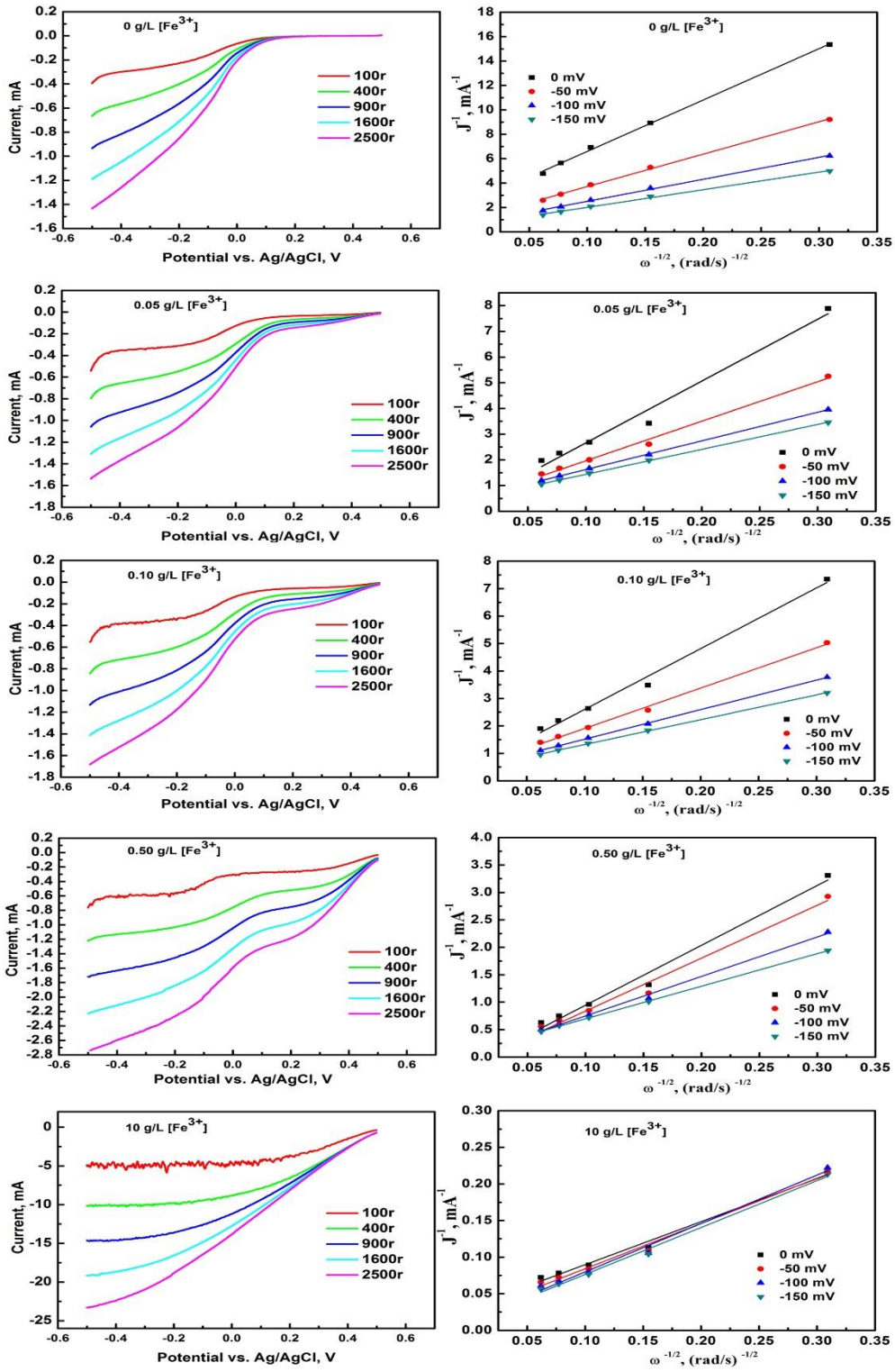

Figure 5. Rotating disk electrode test results for the reduction reaction of dissolved oxygen on pyrite rotating electrode in 0.5 M H_2SO_4 saturated by O_2 at 25 ℃ with a scan rate at 2 mV/s, electrode area: 0.2374 cm^2. The ferric ion content in the electrolyte varied from 0 to 10 g/L (Left figures); Corresponding Koutecky-Levich plots at various potentials: 0 mV, -50 mV, -100 mV and -150 mV respectively according to the data of left figures (Right figures)..

The ETNs shown in Fig. 6 can be illustrated by the above analysis. The Fenton-like reaction is no doubt a multi-electron transferred fast process [23]. Therefore, the intermediates peroxide will be rapidly oxidized to oxygen back and make the oxygen participated in overall oxidation reaction of pyrite material less and less, leading to reduced electrochemical oxidation of pyrite. In this sense, the ETN has a negative correlation to the pyrite oxidation rate. The increasing O_2 reproduction in the reaction (Eq. (17)) with the addition of ferric ions from 0.05 g/L to 10 g/L result in the raising ETN. This also may be one of the reasons why the polarization current increased while the oxygen reduction process was weakened with the addition of ferric ions, as mentioned above.

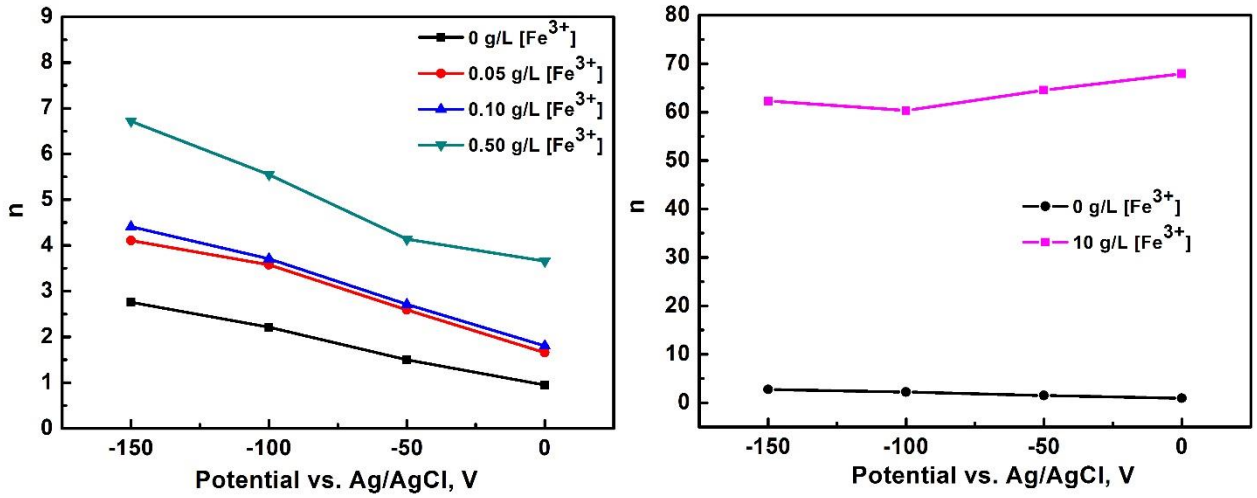

Figure 6. Changes of the electron tranfer numbers for oxygen reductions on natural pyrite at various potentials in the electrolyte adding different ferric ions.

As known from other reports, ferric ions possess strong oxidation properties and can speed up the dissolution of the pyrite sample [9] and formation process of the intermediates peroxide substantially [24]. When a good deal of hydrogen peroxide were produced with the enhancing ferric ion numbers in the electrolyte, the effects not only concludes the weakened dissolved oxygen reduction but also the reactions participated by the pyrite minerals, such as leaching processes of sulphide minerals, froth flotation of pyrite, geochemical element cycling processes and environmental protections.

Previous reports have also provided the experimental test data on the generation of hydroxyl radical [21, 24]. Besides, according to the Eh-pH stability diagram, the products of pyrite oxidation may be ferric oxide or hydroxide in acid media at high solution potential [24]. However, the dissolved oxygen molecular also can form the superoxide during the pH value in the acidic range (Eq. (18, 19)).

$$O_2 + e^- \rightarrow (O_2^{\bullet})^- \quad (18)$$

$$2(O_2^{\bullet})^- + 2H^+ \rightarrow H_2O_2 + O_2 \quad (19)$$

In order to verify the proposed mechanism, a natural pure chalcopyrite electrode was prepared using the similar method to compare with the pyrite electrode. Moreover, a 0.1 g/L silver ion was applied to replace 0.1 g/L ferric ion.

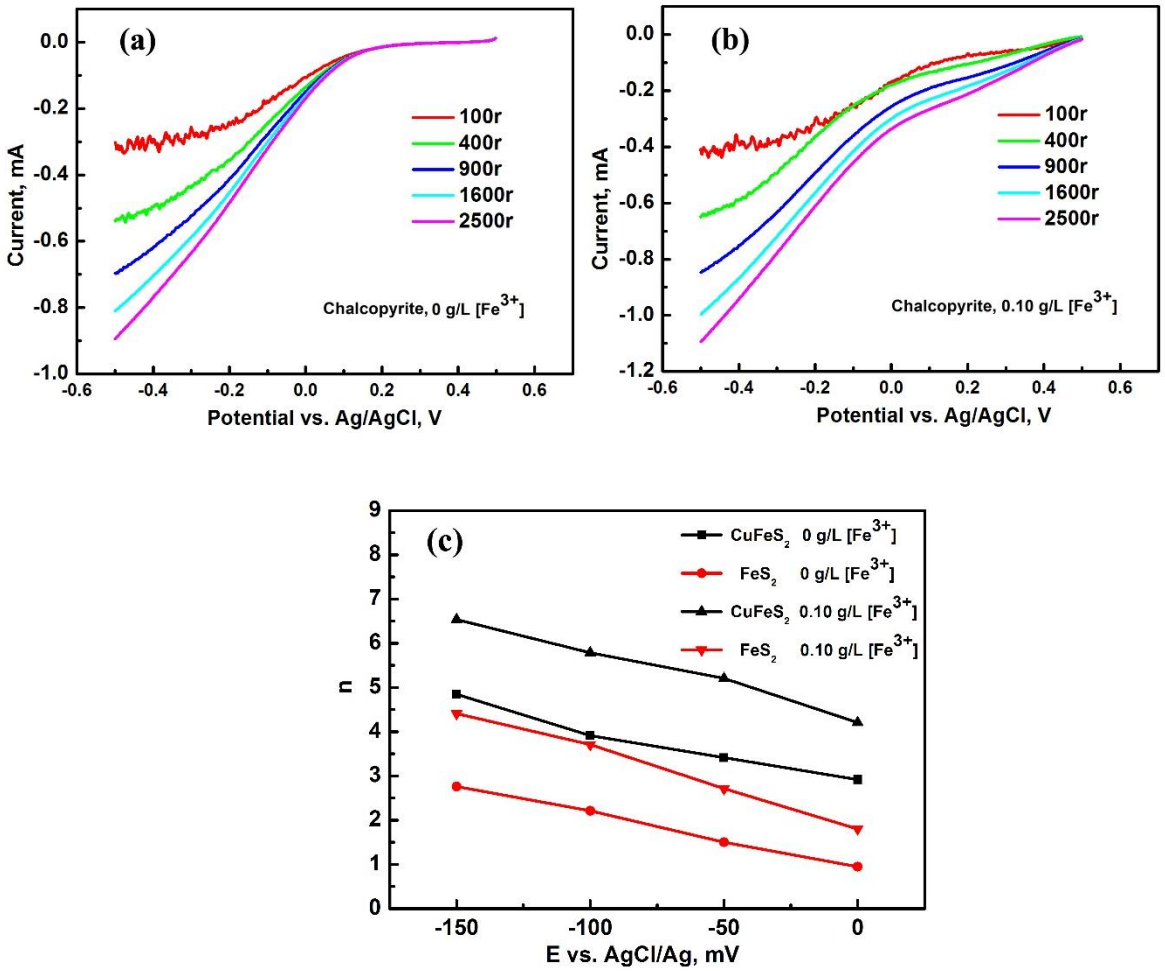

Figure 7. RDE test results and changes of the electron tranfer numbers for oxygen reduction on natural chalcopyrite and pyrite electrodes at various potentials in acidic media. The test conditions were the same with Fig. 5.

The RDE test results and changes of the electron transfer numbers at various potentials in acidic media are shown in Fig. 7 and Fig. 8 respectively. The ETNs were calculated and listed in table 2. It is interesting to find that the addition of ferric ion can also change the electron transfer numbers of chalcopyrite while that of silver ion make little difference from the solution with ferric ions. Besides, the influence of ferric ion on the chalcopyrite electrode is quite similar to the pyrite electrode, comparing our previous researches [25]. Although the initial average electron transfer number for the dissolved oxygen reduction on chalcopyrite was calculated 3.77, near to 4, and the main routes for its oxygen reduction process was experiencing the direct 4e- reduction reaction (Eq. (11)), nevertheless, the Fenton-like reactions (Eq. (15-17)) occurred still after ferric ion was mixed. As a result, the electron transfer number changed accordingly.

In previous studies, hydroxyl radicals are found to be generated from the reaction between silver nanoparticles and H_2O_2 (Eq. (20)) in acidic media [26].

$$H_2O_2 + Ag + H^+ \rightarrow Ag^+ + \bullet OH + H_2O \qquad (20)$$

However, the value of ETN play a decisive role to the electron transfer process. When the ETN value is small (for example, 1-5), the redox potential of silver particles is then between -0.1 and -1.8 V,

a negative number. The result indicates that the silver nanoparticles is a strong electron-donating reagent when reacted with the other compounds, especially inducing the simultaneous oxidation of silver atoms and the production of Ag^+ [27]. In other words, the reaction Eq. (20) is an irreversible reaction, silver ion is difficult to form silver atoms and proceeds the catalytic reaction of hydroxyl radical at this condition. This may be the reason why the electron transfer numbers varied rarely with the increase of silver ion in Fig. 8.

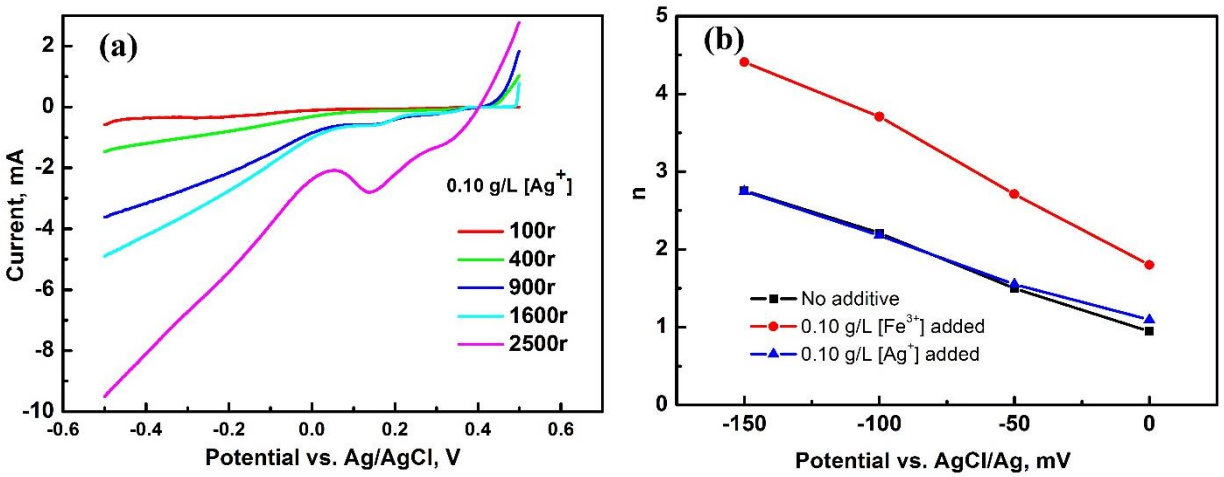

Figure 8. RDE test results and changes of the electron tranfer numbers for oxygen reduction on natural pyrite electrodes at various potentials in 0.10 g/L ferric and silver ions. The test conditions were the same with Fig. 5.

Table 2. The electron tranfer numbers for oxygen reduction in various conditions at different potentials (versus AgCl/Ag electrodes).

Types	$n_{E = -150\ V}$	$n_{E = -100\ V}$	$n_{E = -50\ V}$	$n_{E = 0\ V}$
No additive, Pyrite	2.76	2.21	1.50	0.947
No additive, Chalcopyrite	4.84	3.91	3.41	2.92
0.10 g/L [Fe^{3+}], Pyrite	4.41	3.72	2.71	1.80
0.10 g/L [Ag^+], Pyrite	2.74	2.18	1.55	1.09
0.10 g/L[Fe^{3+}], Chalcopyrite	6.54	5.79	5.21	4.22

4. CONCLUSIONS

In summary, the surface oxidation of natural massive pyrite in 0.5 M sulfuric acid solutions with different ferric ion contents were studied by using electrochemical technologies CV, LSV and RDE methods. From the results, the oxidation process on the pyrite surface took place in the potential range of -0.450 V to 0.050 V vs. AgCl/Ag. It is found that the tafel slopes for the dissolved oxygen reduction increased from 0.354 to 8.04 V/decade when the ferric ions adding into the electrolyte solution. The average ETN for surface oxidation on pyrite in sulfuric acid was near to 2. The increasing of ferric ion was shown to change ETN markedly and inhibit the pyrite electrochemical oxidation. It was ascribed to

the reversible reaction induced by the chemical oxidation. From the comparison of the oxidation behaviors on pyrite with adding silver ions, silver ion is inferred to be difficult to form silver atoms and influence the electrochemical oxidation less.

ACKNOWLEDGEMENTS
This work was supported by the National Key R&D Program of China (2018YFC1902003) and the Fundamental Research Funds for the Central Universities (N172504022).

References

1. A.P. Chandra, and A.R. Gerson, *Surf. Sci. Rep.,* 65 (2010) 293.
2. M. Descostes, P. Vitorge, and C. Beaucaire, *Geochim. Cosmochim. Acta*, 8 (2004) 4559.
3. Y. Mu, Y. Peng, and R.A. Lauten, *Electrochim. Acta*, 174 (2015) 133.
4. A.P. Chandra, and A.R. Gerson, *Geochim. Cosmochim. Acta*, 75 (2011) 6239.
5. Y.J. Xian, Y.J. Wang, and S.M. Wen, *Miner. Eng.,* 72 (2015) 94.
6. M.R. Gao, Y.R. Zheng, and J. Jiang, *Acc. Chem. Res.*, 50 (2017) 2194.
7. P.A., Weber, W.A. Stewart, and W.M., Skinner, *Appl. Geochem.*, 19 (2004) 1953.
8. H.Y. Sun, M. Chen, and L.C. Zou, *Hydrometallurgy*, 155 (2015) 13.
9. A.P. Chandra, and A.R. Gerson, *Geochim. Cosmochim. Acta*, 75 (2011) 6893.
10. C. Heidel, and M. Tichomirowa, *Chem. Geol.*, 281 (2011) 305.
11. M.J. Nicol, H. Miki, and S.C. Zhang, *Hydrometallurgy*, 133 (2013) 188.
12. R. Murphy, and D.R. Strongin, *Surf. Sci. Rep.*, 64 (2009) 1.
13. M.M. Antonijevic, M.D. Dimitrijevic, and S.M. Serbula, *Electrochim. Acta*, 50 (2005) 4160.
14. B.F. Giannetti, S.H. Bonilla, and C.F. Zinola, *Hydrometallurgy*, 60 (2001) 41.
15. Y. Liu, Z. Dang, and P.X. Wu, *Ionics*, 17 (2011) 169.
16. G.H. Kelsall, Q. Yin, and D.J. Vaughan, *J. Electroanal. Chem.*, 471 (1999) 116.
17. D. Majuste, V. Ciminelli, and K. Osseo-Asare, *Hydrometallurgy*, 111 (2012) 114.
18. E. Yeager, *Electrochim. Acta*, 29 (1984) 1527.
19. S. Ye, and A.K. Vijh, *J. Solid State Electrochem.*, 9 (2005) 146.
20. M.S. El-Deab, and T. Ohsaka, *Electrochim. Acta*, 47 (2002) 4255.
21. P. Zhang, S.H. Yuan, and P. Liao, *Geochim. Cosmochim. Acta*, 172 (2016) 444.
22. D.L. Wu, Y.F. Chen, and Y.L. Zhang, *Sep. Purif. Technol.*, 154 (2015) 60.
23. M. Pereira, L. Oliveira, and E. Murad, *Clay Miner.*, 47 (2012) 285.
24. A. Nooshabadi, and K. Rao, *Hydrometallurgy*, 141 (2014) 82.
25. G. Chen, and H.Y. Yang, *Int. J. Electrochem. Sci.*, 11 (2016) 34.
26. D. He, C.J. Miller, and T.D. Waite, *J. Catal.*, 317 (2014) 198.
27. A. Henglein, *J. Chem. Phys.*, 97 (1993) 5457.